An Approximation of Inner Boundary Conditions for Wells Intersecting Highly Conductive Structures

Markus Giese, Thomas Reimann, Rudolf Liedl, Benoît Dewandel, Jean-Christophe Maréchal, Martin Sauter

An Approximation of Inner Boundary Conditions for Wells Intersecting Highly Conductive Structures

by Markus Giese[1], Thomas Reimann[2], Rudolf Liedl[2], Benoit Dewandel[3], Jean-Christophe Maréchal[3], and Martin Sauter[4]

Abstract

Inner boundary conditions describe the interaction of groundwater wells with the surrounding aquifer during pumping and are associated with well-skin damage that limits water production and water derived from wellbore storage. Pumping test evaluations of wells during immediate and early time flow require assignment of inner boundary conditions. Originally, these concepts were developed for vertical well screens, and later transferred to wellbores intersecting highly conductive structures, such as preferential flow zones in fractured and karstic systems. Conceptual models for pumping test analysis in complex bedrock geology are often simplified. Classic analytical solutions generally lump or ignore conditions that limit or enhance well productivity along the well screen at the onset of pumping. Numerical solutions can represent well drawdowns in complex geological settings, such as karst systems, more precisely than many analytical solutions by accounting for additional physical processes and avoiding assumptions and simplifications. Suitable numerical tools for flow simulations in karst are discrete pipe-continuum models that account for various physical processes such as the transient hydraulics of wellbores intersecting highly conductive structures during pumping.

Introduction

Classical well-test interpretation methods are based on conceptual models simplifying the general flow behavior. Usually these theoretical models consist of a basic model, inner and outer boundary conditions (Gringarten 1982). Several analytical solutions are available for various basic models for example, (a) radial flow (Theis 1935), (b) double porosity (Barenblatt et al. 1960; Warren and Root 1963), and (c) single vertical fracture (Papadopulos and Cooper Jr. 1967). These models can be extended by inner boundary conditions, described by various analytical solutions, for example, (d) wellbore storage (Van Everdingen and Hurst 1949; Agarwal et al. 1970) and (e) skin effects (Van Everdingen 1953; Agarwal et al. 1970). Especially in the analysis of wells intersecting highly conductive structures, a detailed considerations of inner boundary conditions representing well losses and/or formation inefficiencies is demanded (Novakowski 1990; Spane Jr and Wurstner 1993). Similarly, outer boundary conditions defining the interaction of the well with catchment heterogeneity on a larger scale can be added. Detailed investigations of outer boundaries effecting flow pattern during pumping are reported by, for example, Walker and Roberts (2003) and Beauheim et al. (2004). Analytical solutions can be combined by the principle of superposition. The resulting pressure or drawdown over time is displayed on a log-log plot, referred to as diagnostic plot (Gringarten 1982). However, complexity increases at early time and adjacent to the well screen.

Pumping from wells intersecting highly conductive structures, such as horizontal wells or fractured aquifers add an additional degree of complexity. A frequently used basic model for drawdown predictions in wellbores intersected by a plane vertical fracture is given by Gringarten et al. (1974). This approach considers two different analytical solutions: (a) infinite conductivity fracture assuming constant pressure along the flow path and (b) uniform flux fracture where the flow per unit fracture surface is assumed to be constant (Gringarten et al. 1974; Bourdet 2002). In general, the pressure drop along uniform flux fractures is low (Gringarten et al. 1974).

[1]Corresponding author: Department of Earth Sciences, University of Gothenburg, Guldhedsgatan 5a, 41320 Göteborg, Sweden; markus.giese@gu.se

[2]Institute for Groundwater Management, TU Dresden, Dresden, Germany, Bergstr. 66, 01069.

[3]NRE, Bureau de Recherches Géologiques et Minières (BRGM), University of Montpellier, 1039 Rue de Pinville, Montpellier, France, 34000.

[4]Geoscientific Centre, University of Göttingen, Goldschmidtstr. 3, Göttingen, Germany, 337077.

The differences between the type curves are therefore marginal and only visible during the transition from linear to radial flow regimes on a diagnostic plot (Bourdet 2002). Fractures without a hydraulic gradient along the fracture can be referred to as an "extension of the well" (Kruseman and de Ridder 1994), which represents the well together with the hydraulically connected productive fracture surface (Jenkins and Prentice 1982).

Van Everdingen (1953) introduced an additional pressure drop referred to as skin effect, as a lumped conceptualization of the effects of water abstraction on well structure and formation inefficiencies (Spane Jr and Wurstner 1993). Wellbore skin is a result of the employed drilling technique (Van Everdingen 1953), particle deposition, or the development of bacterial films (Renard 2006). In general, two different conceptual models of wellbores with skin effects can be formulated (Bourdet 2002): First, damaged wells are characterized by high flow resistance between well and reservoir and, second, stimulated wells have low resistance and increased basic cylindrical vertical wellbore geometry. According to Bourdet et al. (1983), skin effects are visible in the transition or pressure compensation period of highly conductive features and a low conductive reservoir.

Previous studies revealed that within highly conductive structures: (1) flow can be laminar or turbulent, (2) pressure can significantly vary in flow direction and due to the interaction with the surroundings, and (3) discharge varies along the flow direction (Birk et al. 2005; Reimann et al. 2011; Xu et al. 2015; Giese et al. 2018). Because of this complexity, analytical solutions are of limited use due to their inherent limitations. In contrast, various numerical solutions are suitable to reflect pumping from wells that interact with highly conductive structures. The Multi-Node-Well Package (MF-MNW2; Konikow et al. 2009) accounts for skin damage as well as wellbore storage. Exchange flow between highly conductive wellbore and matrix is considered by a well-to-cell conductance term. In MF-MNW2, different input options allow splitting the conductance into terms accounting for different flow restrictions related to numerical and conceptual representation of (horizontal) well segments. However, MF-MNW2 does not account for turbulent flow conditions. The Conduit-Flow-Process 1 for MODFLOW-2005 (CFPM1) is a numerical discrete-continuum model originally developed to simulate karst aquifers (Liedl et al. 2003; Shoemaker et al. 2008). CFPM1 is already used for pumping test evaluation, primarily in karstified systems (cf Reimann et al. 2014; Giese et al. 2017; 2018). However, since CFPM1 is not primarily developed for pumping test analysis, parameters need to be transformed in order to account for wellbore storage and skin. CFPM1 potentially has an advantage over other numerical solutions due to the differentiated pipe-matrix exchange and the ability to consider turbulent flow conditions with possible applications for horizontal wells and hydraulic systems with highly conductive structures. In this paper, CFPM1 is used in an alternative way to represent water abstraction from highly conductive structures. Suitable parameters to reflect wells intersecting highly conductive features are derived. Comparison to analytical solutions for laminar flow conditions prove this approach can be applied for idealized situations. No analytical solutions for turbulent flow conditions were available for comparison. However, the idealized conditions cover a broad value range for different parameters influencing general flow pattern.

Concepts and Solutions

The following section describes the conceptual model of a pumping well that interacts with a highly conductive structure. It presents two approaches to account for the conceptual model: an analytical solution, consisting of a basic model and inner boundary conditions, and a numerical solution that overcome possible limitations of the analytical methods.

Conceptual Model

Skin effect as well as wellbore storage are related to each other. Both influence drawdown, mainly at the beginning of abstraction (McConnell 1993; Park and Zhan 2002). The first period of an abstraction test is normally dominated by storage effects, which create a unit slope on log-log plots (e.g., Ehlig-Economides and Economides 2000; Bourdet 2002). During the storage period, matrix contributions are negligible. With time, the effect of the wellbore storage is reduced and the matrix starts to contribute water (Papadopulos and Cooper Jr. 1967; Schafer 1978). Cinco-Ley and Samaniego-V (1981) applied the skin concept to pumping wells intersected by a single fracture. They describe the effect of different types of damaged wells on drawdown with two conceptual models: (a) choked vertical fracture and (b) fluid loss damage. With fixed wellbore storage, the skin conductance affects the transformation of the drawdown signal from the wellbore to the matrix. Cinco-Ley and Samaniego-V (1981) use the term "fluid loss damaged fracture" for reduced permeability around the fracture that results in an additional pressure loss during transient flow (Figure 1).

Low permeability results in a delayed transformation of the drawdown signal from the wellbore into the matrix. The storage of the skin zone is normally assumed to be infinitesimally small because the actual volume is negligible compared to that of the fissured matrix, resulting

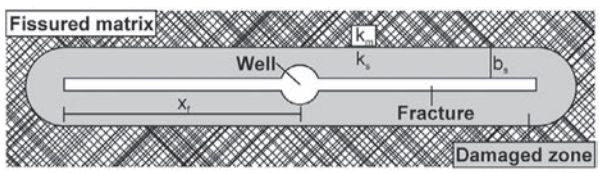

Figure 1. Plan view of a conceptual vertical structure with "quasi"-infinite conductivity and fluid loss damage (after: Cinco-Ley and Samaniego-V 1981): k_m is fissured matrix permeability $[L^2]$, k_s is damaged zone permeability $[L^2]$, x_f is fracture half-length $[L]$, and b_s is damage zone thickness $[L]$.

in a short duration of transformation of the drawdown signal into the matrix (Van Everdingen 1953). Starting with the increased matrix exchange and assuming laminar fracture flow, flow from the adjacent rock to the fracture is perpendicular resulting in linear flow. For later times, in case of an infinite horizontal extension of the aquifer, flow can be described by the general radial flow equation as for any reservoir with infinite horizontal extent (Gringarten 1982).

Analytical Solutions

According to Kruseman and de Ridder (1994), most of the analytical solutions assume an idealized flow domain consisting of an infinite aquifer domain with constant transmissivity. Additionally, initial hydraulic heads are uniform prior to pumping with a constant pumping rate. The dimensionless drawdown along an infinite-conductivity vertical fracture, introduced by a central intersecting pumping well, which also considers effects caused by inner boundary conditions, is defined as (Bertrand and Gringarten 1978)

$$s_D = \frac{\sqrt{\pi t_D}}{2}\left[erf\left(\frac{0.134}{\sqrt{t_D}}\right) + erf\left(\frac{0.866}{\sqrt{t_D}}\right)\right] - 0.067 \cdot Ei\left(-\frac{0.018}{t_D}\right) - 0.433 \cdot Ei\left(-\frac{0.750}{t_D}\right) + S_f \cdot e^{\left(\frac{-t_D}{s_D C_D}\right)} \tag{1}$$

with s_D the dimensionless drawdown [−], t_D the dimensionless time [−], S_f the dimensionless skin damage factor [−], and C_D the dimensionless wellbore storage [−]. The hydraulic properties of the damaged zone can be characterized by the skin damage factor S_f depending only on the ratio of the fissured matrix permeability k_m [L^2] and the damaged zone permeability k_s [L^2] as

$$S_f = \frac{\pi b_s}{2x_f}\left(\frac{k_m}{k_s} - 1\right) \tag{2}$$

with x_f the fracture half-length [L] and b_s the damaged zone thickness [L]; both being constant values (cf Figure 1). In classical pumping test analysis, the skin damage factor S_f is used to explain pressure differences between the wellbore and the adjacent rock that are not caused by the aquifer pressure response.

As an additional tool for the interpretation of pumping tests, the dimensionless drawdown derivative $s_D{}'$ [−] is suitable to detect minor changes in drawdown behavior (Spane Jr and Wurstner 1993) and is defined as (Bourdet et al. 1983)

$$s_D{}' = \frac{\Delta s_D}{\Delta \ln(t_D/C_D)}. \tag{3}$$

Numerical Solutions—Conduit Flow Process in MODFLOW-2005

The discrete pipe-continuum model CFP Mode 1 (CFPM1; Shoemaker et al. 2008) couples one-dimensional (1D) discrete elements (e.g., pipes, conduits) with laminar and turbulent flow to the MODFLOW-2005 continuum simulating laminar Darcian flow (Harbaugh 2005). Laminar pipe flow along the length of the cylindrical pipe segment Δl_p is described by the Hagen-Poiseuille equation as (Shoemaker et al. 2008):

$$Q_p = -\frac{\pi {d_p}^4 g \Delta h_p}{128 \upsilon \Delta l_p \tau} \tag{4}$$

with Q_p the volumetric flow rate [L^3/T], d_p the pipe diameter [L], g the gravitational acceleration [L/T^2], Δh_p the head losses along the pipe [L], υ the kinematic viscosity of water [L^2/T], and τ the tortuosity of the pipe [−]. Exchange flow between the discrete pipe network and the matrix continuum Q_{ex} [L^3/T] is considered by a linear quasi-steady state exchange coefficient α_{ex} [L^2/T] at every pipe node (Barenblatt et al. 1960; Bauer et al. 2003; Shoemaker et al. 2008):

$$Q_{ex} = \alpha_{ex}(h_p - h_m) \tag{5}$$

with h_p the pipe head [L] and h_m the matrix head [L]. According to Bauer et al. (2003), the exchange coefficient α_{ex} is a lumped conductance term representing the geometry of the pipe as well as the properties describing the hydraulic conditions of the interface as

$$Q_{ex} = 2\pi \frac{d_p}{2} \Delta l_p \, \alpha K \tau (h_p - h_m) \tag{6}$$

with K the hydraulic conductivity of the matrix continuum [LT^{-1}] and α the inverse fissure spacing [L^{-1}]. (Reimann et al. 2014) implemented a fast responding storage to the pipe system, which is in direct hydraulic contact with the pipe network:

$$h_{CADS} = h_p \tag{7}$$

with h_{CADS} the hydraulic head in the conduit-associated drainable storage (CADS) [L]. CADS was implemented to provide an additional storage at every pipe node. Changes in hydraulic head in the pipe are directly associated with outflow or inflow from the fast responding storage such as (Reimann et al. 2014)

$$Q_{CADS} = \frac{V_{CADS,t} - V_{CADS,t-\Delta t}}{\Delta t} \tag{8}$$

with

$$V_{CADS} = l_{CADS} W_{CADS} (h_p - z_{Bot}) \tag{9}$$

with l_{CADS} the length of the storage segment associated with the pipe node [L], W_{CADS} the width of the CAD storage [L], and z_{Bot} the elevation of the pipe bottom [L]. The head-related inflow from the storage is immediately available at the pipe node resulting in additional discharge.

Evaluation of Numerical Methods for Pumping Test Analysis of Wells Interacting Highly Conductive Structures

The applied CFPM1 model setup is appropriate to fulfill the requirements of an idealized aquifer. A large extent of the model domain (113,000 m × 113,000 m) is suitable to represent a quasi-infinite aquifer by avoiding boundary effects. The uniform aquifer thickness is $b = 250$ m with a bottom elevation of 0 m. The matrix is considered as a single confined layer with initial hydraulic heads of 500 m. The storativity of the layer is $S = 2.5 \cdot 10^{-2}\,\mathrm{m}^{-1}$ and the transmissivity $T = 2.5 \cdot 10^{-2}\ \mathrm{m}^2/\mathrm{s}$. The following setups consider a single straight pipe with varying length. The pumping well (Neumann boundary condition), with a constant pumping rate of $Q_p = 0.5\,\mathrm{m}^3/\mathrm{s}$, is centrally located in the pipe as well as in the model domain. The pumping time is suited to investigate hydraulic effects of inner boundary conditions on drawdown immediately after commencement of pumping. Each pipe consists of a defined number of pipe nodes which are connected by pipe sections each of length $\Delta l = 20$ m and pipe diameter $d_p = 1$ m. Due to the limitation of most analytical solutions, that is, "quasi"-infinite pipe conductivity, the pipe flow is simulated by the Hagen-Poiseuille equation, applicable for laminar flow conditions. The setup uses a stepwise increase of the spatial discretization of the model domain from 1 m directly at the pipe to a cell size of 100 m.

Calculation of Dimensionless Drawdown for Numerical Models

For the comparison of pumping test results, dimensionless parameters are used to erase the influence of different hydraulic properties or different pumping rates on well drawdown. For a well intersecting a planar fracture in a homogeneous, isotropic and confined aquifers, the dimensionless parameters can be defined as (Bertrand and Gringarten 1978; Spane Jr and Wurstner 1993)

$$s_D = \left(\frac{2\pi T}{Q_p}\right)\Delta s \tag{10}$$

$$C_D = \frac{C}{2({x_f}^2 S\pi)} \tag{11}$$

$$t_D = \frac{Tt}{{x_f}^2 S} \tag{12}$$

with Δs the water-level change inside the fracture [L], C the wellbore storage constant [L^2], T the matrix transmissivity [L^2T^{-1}], and S the matrix storativity [$-$]. In order to compare with the analytical dimensionless drawdown, these equations are used to convert the drawdown computed by CFPM1.

Parameter Transformation—Skin Damage Factor

According to equation 5, CFPM1 uses the exchange coefficient α_{ex} to regulate the exchange flow between aquifer matrix and wellbore. Therefore, the exchange coefficient accounts for pressure head differences between matrix and pipe. Similar to the exchange coefficient of CFMP1, MF-MNW2 considers a well-to-cell hydraulic conductance term CWC [L^2T] (Konikow et al. 2009)

$$Q_{ex} = CWC\,(h_p - h_m). \tag{13}$$

The hydraulic conductance consist of different terms. A linear aquifer-loss coefficient A is used for the determination of exchange flow between matrix cell and wellbore node. This coefficient accounts for cell-to-well head losses for finite-differences models and is a function of the ratio of the cell size (effective external radius, r_o [L]) and the pipe diameter r_w [L]. The aquifer-loss coefficient is defined as (Konikow et al. 2009):

$$A = \frac{\ln\left(\frac{r_o}{r_w}\right)}{2\pi b\ \overline{K_x K_y}} \tag{14}$$

with

$$r_0 = 0.28\frac{\sqrt{\Delta x^2\sqrt{\frac{K_y}{K_x}} + \Delta y^2\sqrt{\frac{K_x}{K_y}}}}{\sqrt[4]{\frac{K_y}{K_x}} + \sqrt[4]{\frac{K_x}{K_y}}} \tag{15}$$

with b the saturated thickness of the cell [L], K the hydraulic conductivity [LT], and Δx, Δy the grid spacing in x and y direction [L]. This term only accounts for steady-state flow neglecting head losses resulting from skin effects and local turbulence (Konikow et al. 2009). The linear well-loss coefficient B quantifies head losses at the interface between the wellbore and the matrix, for example, formation damages or gravel packs and can be defined as (Konikow et al. 2009)

$$B = \frac{S_f}{2\pi K\,\Delta l} \tag{16}$$

Linear aquifer-loss and linear well-loss coefficient are applied as conductance in Figure 2. Two different drawdown curves of the numerical model are presented: (1) the linear well-loss coefficient B individually ($A = 0$) and (2) a combination of aquifer-loss coefficient and linear well-loss coefficient ($\alpha_{ex} = A + B$). Dimensionless drawdown computed for different skin damage factors ($S_f = 1$ to $S_f = 0.001$) by the analytical solution (Equation 1) and the numerical model are compared. The applied parameter values are presented in Table 1.

The numerical model is not able to represent the analytical drawdown behavior. Differences in drawdown are especially high for high skin damage factors (Figure 2a and 2b). The drawdown curves of the computed exchange coefficient, considering only the linear well-loss coefficient B, underestimate drawdown at the beginning of pumping. For a skin damage value of $S_f = 1$ (Figure 2a) both numerical solutions underestimate drawdown compared to the analytical solution. In all cases, the drawdown of the combined coefficients ($A + B$) is approximately

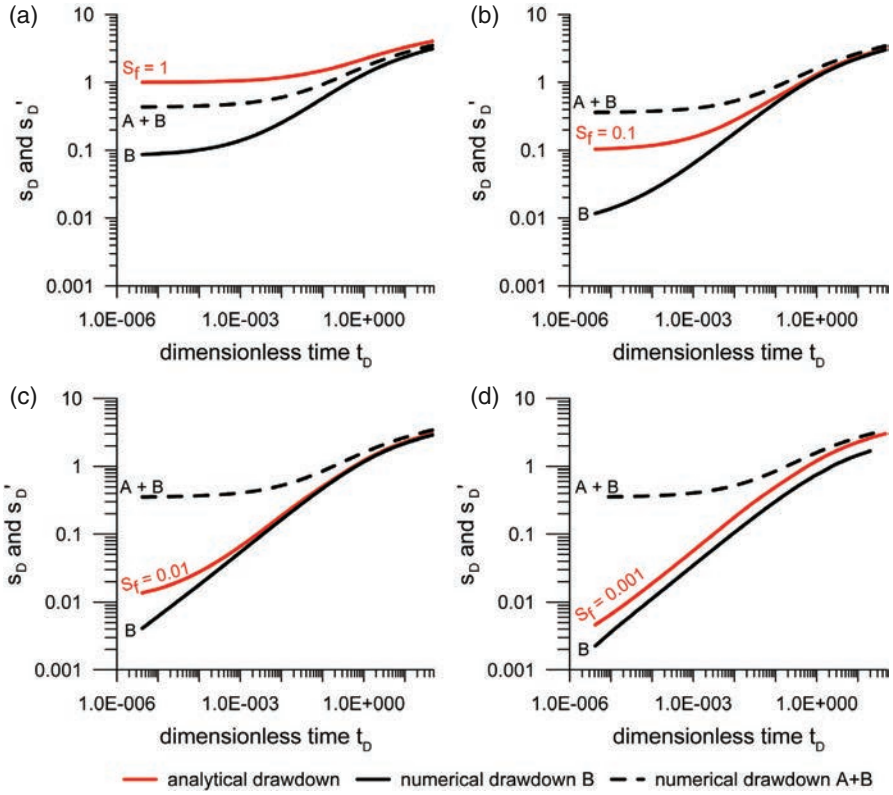

Figure 2. Comparison of the analytical and the numerical drawdown behavior for (a) $S_f = 1$, (b) $S_f = 0.1$, (c) $S_f = 0.01$, and (d) $S_f = 0.001$ without the consideration of wellbore storage.

Table 1
Parameter Values for the Exchange Coefficient Terms for a Hydraulic Conductivity $K = 1.0 \cdot 10^{-4}$ m/s (According to Equation 14 and Equation 16)

S_f [−]	A [s/m^2]	B [s/m^2]	$A+B$ [s/m^2]
1.0	338.09	79.58	$2.39 \cdot 10^{-3}$
$1.0 \cdot 10^{-1}$	338.09	7.96	$2.89 \cdot 10^{-3}$
$1.0 \cdot 10^{-2}$	338.09	$7.96 \cdot 10^{-1}$	$2.95 \cdot 10^{-3}$
$1.0 \cdot 10^{-3}$	338.09	$7.96 \cdot 10^{-2}$	$2.96 \cdot 10^{-3}$

equal. The minor changes are due to changes of the linear well-loss coefficient B, since the aquifer-loss coefficient A is constant (cf Table 1). This is the consequence of the applied setup with one single layer of 250-m thickness in the two-dimensional (2D) domain. The cell thickness is by far the largest cell side and according to Equation 15 the computed effective external radius ($r_o = 35$ m) exceeds the pipe diameter ($d_p/2 = 0.5$ m). The linear aquifer-loss coefficient is constant, as long as the discretization of the model domain and pipe remain unchanged. The well-loss coefficient is linearly related to the skin damage factor. By increasing the skin damage factor S_f by one order of magnitude, the linear well-loss coefficient B increases by the same magnitude (Table 1).

In consequence of the previously describes deficits, an additional pressure term needs to be included to counterbalance the influence of the linear aquifer-loss coefficient. Therefore, the reciprocal exchange coefficient will be expanded by an empirical calibration coefficient (ECC) as

$$\alpha_{ex} = (A + B + ECC) \tag{17}$$

In this analysis, the ECC might also allow for effects caused by different functioning and geometries (plane fracture vs. cylinder with finite volume) as well as different representations of the skin and the computation of the drawdown along the half-fracture length. The analytical solution integrates the drawdown along the half-fracture length instead of computing a single value per unit length. The initial exchange coefficient value needs to be calibrated with respect to the analytically calculated drawdown. This can be done manually (this study) or by a calibration tool, for example, PEST (Doherty 2015). The calibration needs to be conducted for one skin damage factor only.

Parameter Transformation—Dimensionless Wellbore Storage

The wellbore storage constant C [L^2] is a function of the casing radius and defined as (Moench 1984; Novakowski 1990)

$$C = {r_c}^2 \pi \tag{18}$$

where r_c is the well casing radius [L]. The casing radius describes the area affected by hydraulic head changes

Table 2
Parameter Values for the Three Exchange Coefficient Terms (According to Equation 17)

	S_f [−]	Factor	α_{ex} [m²/s]	A [s/m²]	B [s/m²]	ECC [s/m²]
$K = 1.0{\cdot}10^{-5}$ m/s	1.0	$1.0{\cdot}10^{-1}$	$1.07{\cdot}10^{-4}$	3380.85	795.77	183,064.74
	$1.0{\cdot}10^{-1}$		$1.07{\cdot}10^{-3}$		79.58	15,263.71
	$1.0{\cdot}10^{-2}$		$1.07{\cdot}10^{-2}$		7.96	−1516.39
	$1.0{\cdot}10^{-3}$		$1.07{\cdot}10^{-1}$		$7.96{\cdot}10^{-1}$	−3194.41
$K = 1.0{\cdot}10^{-3}$ m/s	1.0	$1.0{\cdot}10^{1}$	$1.07{\cdot}10^{-2}$	33.80	7.96	1830.00
	$1.0{\cdot}10^{-1}$		$1.07{\cdot}10^{-1}$		$7.96{\cdot}10^{-1}$	152.64
	$1.0{\cdot}10^{-2}$		1.07		$7.96{\cdot}10^{-2}$	−15.16
	$1.0{\cdot}10^{-3}$		10.68		$7.96{\cdot}10^{-3}$	−31.94
$M = 50$ m	1.0	$2.0{\cdot}10^{-1}$	$2.14{\cdot}10^{-4}$	210.03	79.58	93,331.08
	$1.0{\cdot}10^{-1}$		$2.14{\cdot}10^{-3}$		7.96	9144.09
	$1.0{\cdot}10^{-2}$		$2.14{\cdot}10^{-2}$		$7.96{\cdot}10^{-1}$	725.39
	$1.0{\cdot}10^{-3}$		$2.14{\cdot}10^{-1}$		$7.96{\cdot}10^{-2}$	−116.48
$M = 25$ m	1.0	$1.0{\cdot}10^{-1}$	$1.07{\cdot}10^{-4}$	154.91	79.58	187,006.86
	$1.0{\cdot}10^{-1}$		$1.07{\cdot}10^{-3}$		7.96	18,561.27
	$1.0{\cdot}10^{-2}$		$1.07{\cdot}10^{-2}$		$7.96{\cdot}10^{-1}$	1716.70
	$1.0{\cdot}10^{-3}$		$1.07{\cdot}10^{-1}$		$7.96{\cdot}10^{-2}$	32.25
$x_f = 500$ m	1.0	$3.4{\cdot}10^{-1}$	$3.10{\cdot}10^{-3}$	338.09	79.58	6033.95
	$1.0{\cdot}10^{-1}$		$3.10{\cdot}10^{-2}$		7.96	299.12
	$1.0{\cdot}10^{-2}$		$3.10{\cdot}10^{-1}$		$7.96{\cdot}10^{-1}$	−274.36
	$1.0{\cdot}10^{-3}$		3.10		$7.96{\cdot}10^{-2}$	−331.71
$x_f = 100$ m	1.0	$7.4{\cdot}10^{-2}$	$1.44{\cdot}10^{-2}$	338.09	79.58	971.23
	$1.0{\cdot}10^{-1}$		$1.44{\cdot}10^{-1}$		7.96	−207.15
	$1.0{\cdot}10^{-2}$		1.44		$7.96{\cdot}10^{-1}$	−324.99
	$1.0{\cdot}10^{-3}$		14.4		$7.96{\cdot}10^{-2}$	−324.28

leading to wellbore storage (Moench 1984). According to Cinco-Ley et al. (1978), the same effect as caused by wellbore storage can be created by the storage of a highly conductive fracture. The circular area (surrounding the vertical wellbore) describes the same area as the horizontal CAD-storage (Equation 9). Therefore, the casing radius for highly conductive pipes, assuming only minor pressure drops along the pipe, can be described as a function of the CAD-storage as

$$r_c = \sqrt{\frac{\sum(l_{CADS} W_{CADS})}{\pi}} \tag{19}$$

McConnell (1993) describes an increase in wellbore storage by a factor of 10 to 100 for wellbores intersected by fractures compared to unfractured wellbores. Joints, faults, and fissures only add a marginally proportion of porosity to the wellbore storage (Worthington et al. 2000; Bourdet 2002).

Comparison of Results and Discussion

Skin Damage Factor

The composition of the exchange coefficient according to Equation 17 and the influence on drawdown caused by the three exchange terms will be further analyzed. Table 2 lists the applied parameters and the exchange term values.

According to Equation 5 and 6, the exchange coefficient α_{ex} is a linear function of the matrix hydraulic conductivity K. Furthermore, the hydraulic matrix conductivity is part of the linear aquifer-loss as well as the linear well-loss coefficient. According to Equations 14 and 16, the change of the two terms is reciprocal to the hydraulic conductivity. Hence, the ratio between the three exchange terms stays constant by changing the hydraulic matrix conductivity. Figure 3a and 3b presents a reasonable match between the analytically and the numerically computed drawdown for all applied skin damage factors. Drawdown differences are generally low during the entire pumping period. The drawdown behavior reflects the commencement of the transition period between linear and radial flow approximately at $t_D = 0.1$ very well. The dimensionless residuals confirm the overall small discrepancies between analytical solution and the result of CFPM1. Differences are low for a hydraulic conductivity of $K = 1.0 \cdot 10^{-5}$m/s. For a hydraulic conductivity of $K = 1.0 \cdot 10^{-3}$m/s, the dimensionless residuals are low at the beginning and increase at approximately $t_D = 0.05$. This time level indicates the start of the transition period. The drawdown difference during the transition period can be explained by different flow behavior, visible in the shape of the derivative curve shown in Figure 3b (and even more pronounced in Figure 3f). The analytical drawdown curve increases steeply, resulting in a shallow slope of the derivative curve and hence positive residual values during this period. Those differences can be explained by the slightly earlier start of Darcy flow conditions in the analytical solution. Nevertheless, the

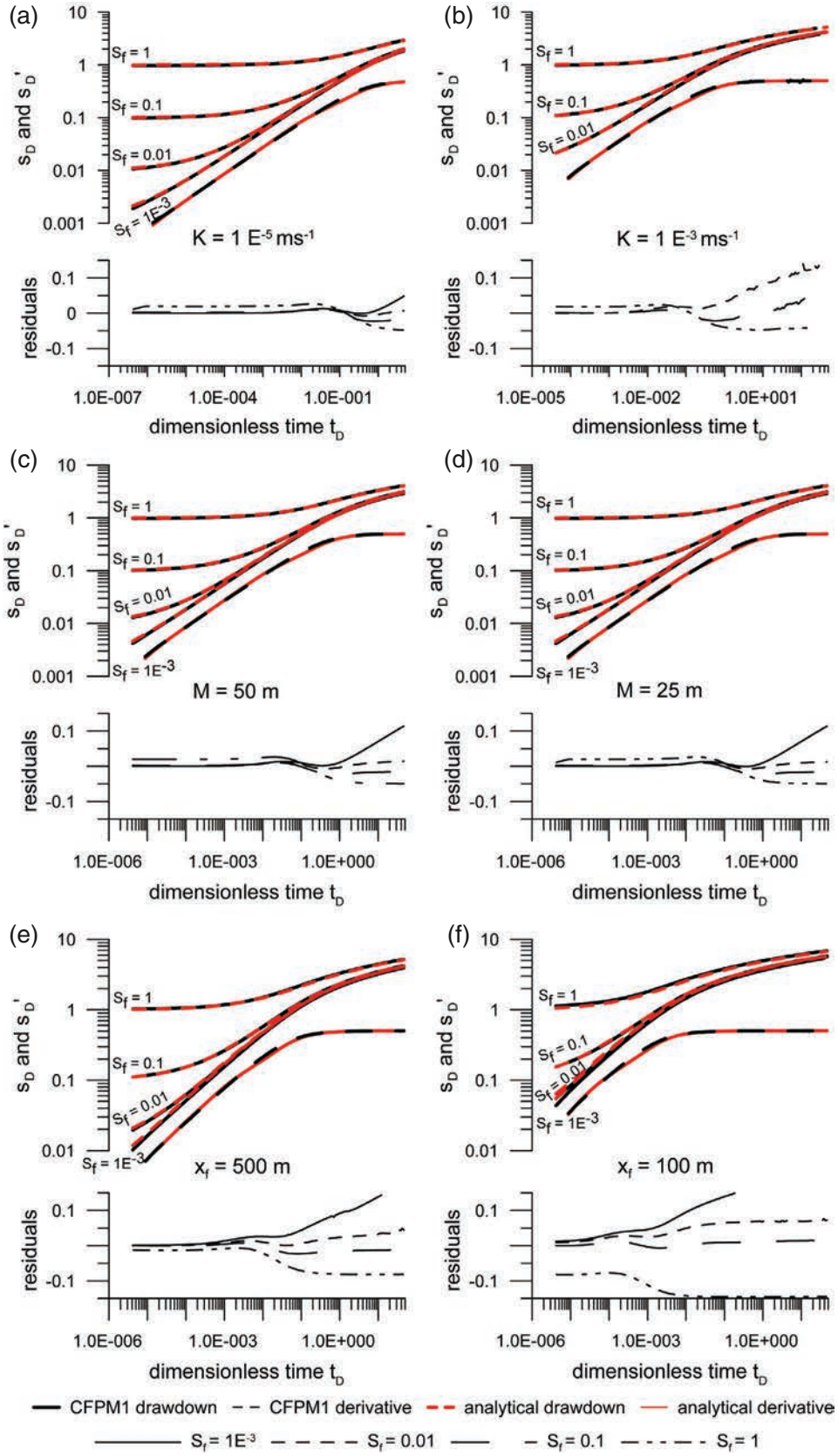

Figure 3. Comparison of analytical and numerical drawdown for different skin damage values in terms of dimensionless drawdown, derivative, and residuals for (a) a hydraulic conductivity of $K = 1.0 \cdot 10^{-5}$ m/s, (b) a hydraulic conductivity of $K = 1.0 \cdot 10^{-3}$ m/s, (c) a layer thickness of $M = 50$ m, (d) a layer thickness of $M = 25$ m, (e) a pipe half-length of $x_f = 500$ m, and (f) a pipe half-length of $x_f = 100$ m without the consideration of wellbore storage.

relative error caused by the drawdown discrepancy is less than 5%. In Figure 3b, the drawdown curves for the skin damage factor of $S_f = 1.0 \cdot 10^{-3}$ are not presented because of numerical instability of the CFPM1 model.

The thickness of the confined layer changes the transmissivity of the model domain. The thickness, and therefore the transmissivity, is not part of the exchange coefficient according to Equation 6. According to Equation 14, the exchange coefficient is linearly related to the matrix transmissivity. The thickness of the layer changes the linear aquifer-loss coefficient A due to the decrease in layer thickness, which is one of the cell edges. The linear well-loss coefficient stays constant for the relative skin damage factors. The applied exchange coefficient, adjusted by the factor of 0.2 and 0.1 (M_{ini} /M_{new}) for a layer thickness of $M = 50\,\text{m}$, respectively, $M = 25\,\text{m}$, approximates the analytical drawdown adequately (Figure 3c and 3d). The dimensionless residuals are small for the entire pumping period and, therefore, is the accuracy of the drawdown comparable to the one presented in Figure 3a and 3b.

The pipe half-length x_f is neither part of the exchange coefficient nor of one of the two linear loss coefficients. Therefore, the values of A and B do not change, while the exchange coefficient differs from the initial one. The changing factor cannot be directly calculated, thus the exchange coefficient needs to be recalibrated. Figure 4 presents the calibration results for a half-pipe length of $x_f = 10\,\text{m}$ up to $x_f = 1500\,\text{m}$ for the introduced setup. The results can be approximated by a potential function. For the presented half-pipe lengths, a log-log linearized function describes the relationship between the exchange coefficient α_{ex} and the skin damage factor. With decreasing half-pipe length, the drawdown difference between small skin values assimilates and the differentiation of skin values becomes difficult (Figure 3f). Differences between analytical and numerical drawdowns increase for the given setup. One reason is the already mentioned differences in flow pattern during the transition period, starting early for short pipe half-length configurations. An adjustment of the spatial discretization with finer cell sides in horizontal as well as vertical direction could buffer the discrepancy and is highly recommended for modeling case studies at local scale.

In sum, the exchange coefficient α_{ex} is able to represent the analytical transient drawdown curve of a well intersecting a highly conductive structure in consideration of skin damage. The analysis shows that the exchange coefficient is related to the spatial discretization of the control volume as well as to the hydraulic and geometric parameters describing the model domain and therefore the entire flow system.

Dimensionless Wellbore Storage

The fast-responding pipe storage of a single pipe describes the same area affected by the casing radius defined for vertical wellbores (Equation 19). To verify the equation, different CADS-widths are compared to different casing radii of the analytical solution (Equation 1).

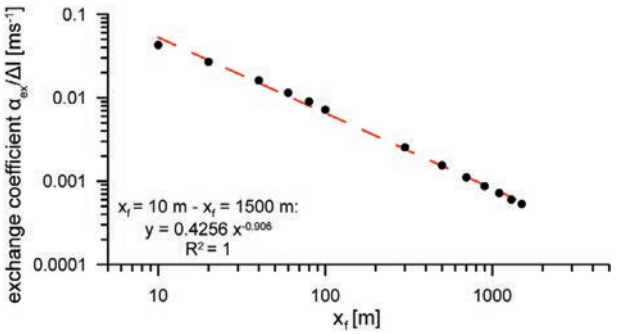

Figure 4. Calibration curve for the exchange coefficient α_{ex} per unit length Δl related to the half-pipe length for a parameter range of $x_f = 10\,\text{m}$ up to $x_f = 1500\,\text{m}$.

Table 3
Parameter Values for the Calculation of the Dimensionless Wellbore Storage

r_c [m]	W_{CADS} [m]	C [m^2]	C_D [−]
2.5	0.007	19.63	$5.6 \cdot 10^{-5}$
5.0	0.026	78.54	$2.2 \cdot 10^{-5}$
10.0	0.105	314.16	$8.9 \cdot 10^{-4}$
15.0	0.654	706.86	$2.0 \cdot 10^{-3}$

The values of the different storage representations are listed in Table 3. Figure 5 shows diagnostic plots of analytically calculated drawdown curves for different casing radii (Equation 1) that are compared to numerically computed drawdowns for corresponding W_{CADS} values (Equation 19). Both the analytical and the numerical representation of the pipe assume a half-length $x_f = 1{,}500\,\text{m}$, a pipe diameter of $d_p = 1.0\,\text{m}$ and a skin factor of $S_f = 1.0$.

The casing radius (pipe storage) only influences the shape of the drawdown curves at the start of pumping. During this period, all the different parameterizations show a linear unit slope in the diagnostic plots indicating wellbore storage effects. With increasing casing radius, drawdown decreases at early times and the water stored in the well provides the major part of the abstracted volume. Because of the low hydraulic gradient between pipe and fractured matrix, the exchange flow is negligible at the beginning of water abstraction. During the transition period, that is, when the matrix starts to contribute water to the pipe system, the derivative shows a characteristic change in slopes. After the storage and the transition period, the drawdown curves for all the setups show a similar behavior, which can be described by linear flow equations.

The numerically computed drawdown curve matches the analytically calculated one (Figure 5). The residuals between analytical and numerical drawdown are close to zero during the entire storage period. The highest drawdown differences can be detected during the transition between storage and linear flow period. The differences

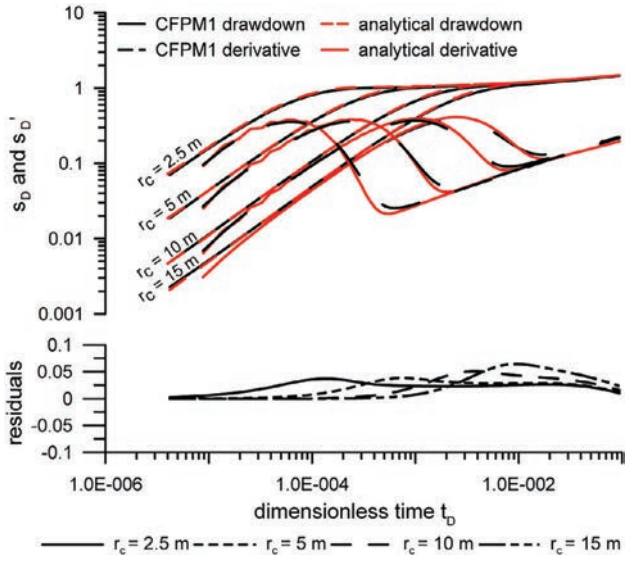

Figure 5. Representation of dimensionless wellbore storage computed by CFPM1 (black curves) and the analytical solution (red curves) for a skin damage factor of $S_f = 1$.

are also visible at the derivative curves. The residuals start to increase at the end of the storage effect dominated period. During the transition to linear flow, the discrepancy increases resulting in a significant change in slopes just before reaching the linear flow period. The pipe drawdown is underestimated by the numerical model, which can be explained by the effect of well storage. The discrepancy between the two solutions increases with growing wellbore storage. The discrete numerical model starts the transition period slightly faster than predicted by the analytical solution. Therefore, the increased exchange dampens the drawdown compared to the time step predicted by the analytical solution.

Conclusions

The above analysis shows that the discrete pipe-continuum model CFPM1, together with the introduced equations are able to simulate the inner boundary conditions, that is, wellbore storage and skin effects in a wellbore-fractured aquifer configuration over a large parameter space. The drawdown of a planar and vertical fracture derived by an analytical solution can be approximated with reasonable accuracy. An equation is presented to consider wellbore storage by the fast-responding storage of CFPM1. Furthermore, the relationship between the analytical skin damage factor and the numerical exchange coefficient, frequently applied for source/sink terms in different MODFLOW packages (e.g., MF-MNW2), is analyzed.

The analysis is limited to a single layer model, but presents the dualism of the exchange coefficient. As long as the ECC cannot be defined, the parameter serves as a calibration parameter. However, the results show that the calibration needs to be executed only once unless the spatial discretization of the model domain is changed. Afterwards, assuming a constant spatial discretization as well as a constant well screen length, the exchange coefficient only has to be adjusted manually, for example, for the analysis on the effect of skin changes on general flow pattern. The discrimination of the drawdown effects caused by different exchange terms also has the advantage that further processes, that is, clogging, iron hydroxide deposition, resulting in localized pressure differences between pipe and matrix, can be included in the numerical model.

The setup of the analyses is primarily chosen to represent idealized conditions during pumping tests in karst aquifer systems. These results can be used for the interpretation of pumping tests in mature karst systems characterized by highly conductive features, for example, solution enlarged fractures, conduits, and caves. For this purpose, one further enhancement of the exchange coefficient can be the implementation of non-linear exchange flow. Based on the analogy with the concept of representing horizontal wellbores, CFPM1 can be applied for the analysis of pumping tests in horizontal wells. In contrast to analytical solutions, CFPM1 provides the advantage of a discrete parameterization of pipe segments and/or the capability to consider turbulent flow.

For the application of the discrete pipe-continuum model CFPM1 to the interpretation of horizontal well tests further expansions and studies are required. The approach presented here currently only allows for quasi-infinite conductivity along the pipe. Due to the smaller diameter of horizontal wellbores, this type of flow regime is unlikely to prevail in horizontal wells (Giese et al. 2018), especially taking the technical inventions during the last decades into consideration. With increased abstraction rate and increased length of the well screen, changes in flow regimes can occur. These changes can be caused by transition zones of laminar and turbulent flow inside as well as nonuniform skin zones in the annulus adjacent to the well. This questions the validity of the assumption of an infinite conductivity and uniform flux solutions for horizontal wellbores (Ozkan 2002). Due to the coupling concept of discrete features to a matrix continuum, pumping test analyses of horizontal wells with unsteady inner boundary conditions and the prediction of resulting flow field changes are possible.

Acknowledgments

The authors thank Eve Kuniansky and Wayne Barclay Shoemaker for their constructive comments that helped to improve the manuscript. This project was funded by the Deutsche Forschungsgemeinschaft (DFG) under grants no. LI 727/11-2 and GE 2173/2-2 and by the BRGM under grants no. PDR13D3E91 and PDR14D3E61. All input data for the CFPM1 are available for download (zenodo): https://doi.org/10.5281/zenodo.3374617.

Authors' Note

The author(s) does not have any conflicts of interest.

References

Agarwal, R.G., R. Al-Hussainy, and H. Ramey Jr. 1970. An investigation of wellbore storage and skin effect in unsteady liquid flow: I. Analytical treatment. *Society of Petroleum Engineers Journal* 10, no. 03: 279–290.

Barenblatt, G., I.P. Zheltov, and I. Kochina. 1960. Basic concepts in the theory of seepage of homogeneous liquids in fissured rocks [strata]. *Journal of Applied Mathematics and Mechanics* 24, no. 5: 1286–1303.

Bauer, S., R. Liedl, and M. Sauter. 2003. Modeling of karst aquifer genesis: Influence of exchange flow. *Water Resources Research* 39, no. 10.

Beauheim, R.L., R.M. Roberts, and J.D. Avis. 2004. Well testing in fractured media: Flow dimensions and diagnostic plots. *Journal of Hydraulic Research* 42, no. S1: 69–76.

Bertrand, L. and A. Gringarten. 1978. Détermination des caractéristiques hydrauliques des aquiféres fissurés par pompage d'essai en régime transitoire—Application aux nappes de la craie. Final report 78 SGN 669 GEG, BRGM Orléans.

Birk, S., T. Geyer, R. Liedl, and M. Sauter. 2005. Process-based interpretation of tracer tests in carbonate aquifers. *Groundwater* 43, no. 3: 381–388.

Bourdet, D. 2002. *Well Test Analysis: The Use of Advanced Interpretation Models*, Vol. 3. Amsterdam: Elsevier.

Bourdet, D., T. Whittle, A. Douglas, and Y. Pirard. 1983. A new set of type curves simplifies well test analysis. *World Oil* 196, no. 6: 95–106.

Cinco-Ley, H., and F. Samaniego-V. 1981. Transient pressure analysis for fractured wells. *Journal of petroleum technology* 7490: 1749–1766.

Cinco-Ley, H., F. Samaniego-V, and N. Dominguez-A. 1978. Transient pressure behaviour for a well with a finite-conductivity vertical fracture. *Journal of petroleum technology* 6014: 253–264.

Doherty, J. 2015. Calibration and uncertainty analysis for complex environmental models: PEST—Complete theory and what it means for modelling the real world. Watermark, Brisbane, watermark numerical computing edition.

Ehlig-Economides, C.A., and M. Economides. 2000. Formation characterization: Well and reservoir testing. In *Reservoir Stimulation*, 3rd ed, ed. M.J. Economides and K.G. Nolte, 2-1–2-25. New York: Wiley.

Giese, M., T. Reimann, V. Bailly-Comte, J.-C. Maréchal, M. Sauter, and T. Geyer. 2018. Turbulent and laminar flow in karst conduits under unsteady flow conditions: Interpretation of pumping tests by discrete conduit-continuum modeling. *Water Resources Research* 54, no. 3: 1918–1933.

Giese, M., T. Reimann, R. Liedl, J.-C. Maréchal, and M. Sauter. 2017. Application of the flow dimension concept for numerical drawdown data analyses in mixed-flow karst systems. *Hydrogeology Journal* 25, no. 3: 799–811.

Gringarten, A. 1982. Flow—Test evaluation of fractured reservoirs. *Geological Society of America Special Papers* 189: 237.

Gringarten, A.C., H.J. Ramey Jr., and R. Raghavan. 1974. Unsteady-state pressure distributions created by a well with a single infinite-conductivity vertical fracture. *Society of Petroleum Engineers Journal* 14, no. 04: 347–360.

Harbaugh, A. 2005. Modflow-2005, the U.S. geological survey modular ground-water model—The ground-water flow process. *U.S. Geological Survey Techniques and Methods*: 6–A16.

Jenkins, D.N., and J.K. Prentice. 1982. Theory for aquifer test analysis in fractured rocks under linear (nonradial) flow conditions. *Groundwater* 20, no. 1: 12–21.

Konikow, L.F., G.Z. Hornberger, K.J. Halford, and R.T. Hanson. 2009. Revised multi-node well (MNW2) package for modflow ground-water flow model. *US Geological Survey Techniques and Methods*: 6–A30.

Kruseman, G.P., and N.A. de Ridder. 1994. *Analysis and Evaluation of Pumping Test Data*, 2nd ed. Wageningen, the Netherlands: International Institute for Land Reclamation and Improvement. (completely rev.), reprint. edition.

Liedl, R., M. Sauter, D. Hückinghaus, T. Clemens, and G. Teutsch. 2003. Simulation of the development of karst aquifers using a coupled continuum pipe flow model. *Water Resources Research* 39, no. 3.

McConnell, C. 1993. Double porosity well testing in the fractured carbonate rocks of the ozarks. *Groundwater* 31, no. 1: 75–83.

Moench, A. 1984. Double-porosity model for a fissured groundwater reservoir with fracture skin. *Water Resources Research* 20, no. 7: 831–846.

Novakowski, K.S. 1990. Analysis of aquifer tests conducted in fractured rock: A review of the physical background and the design of a computer program for generating type curves. *Groundwater* 28, no. 1: 99–107.

Ozkan, E. 2002. Analysis of horizontal-well responses: Contemporary vs. conventional. *SPE Reservoir Evaluation Engineering* 4, no. 4: 260–269.

Papadopulos, I.S., and H.H. Cooper Jr. 1967. Drawdown in a well of large diameter. *Water Resources Research* 3: 241–244.

Park, E., and H. Zhan. 2002. Hydraulics of a finite-diameter horizontal well with wellbore storage and skin effect. *Advances in Water Resources* 25: 389–400.

Reimann, T., M. Giese, T. Geyer, R. Liedl, J.-C. Maréchal, and W.B. Shoemaker. 2014. Representation of water abstraction from a karst conduit with numerical discrete-continuum models. *Hydrology and Earth System Sciences* 18, no. 1: 227–241.

Reimann, T., C. Rehrl, W.B. Shoemaker, T. Geyer, and S. Birk. 2011. The significance of turbulent flow representation in single-continuum models. *Water Resources Research* 47, no. 9.

Renard, P. 2006. Hydraulics of wells and well testing. In *Encyclopedia of Hydrological Sciences, Part 13: Groundwater*. New York: Wiley Online Library.

Schafer, D.C. 1978. Casing storage can affect pumping test data. *Johnson Drillers' Journal*, Jan/Feb, Johnson Division, UOP, Inc., St. Paul, Minnesota.

Shoemaker, W.B., E.L. Kuniansky, S. Birk, S. Bauer, and E.D. Swain. 2008. Documentation of a conduit flow process (CFP) for MODFLOW-2005. In *US Geological Survey Techniques and Methods, Book 6, Chapter A24*. US Geological Survey: Reston, Virginia.

Spane, F.A. Jr., and S.K. Wurstner. 1993. Deriv: A computer program for calculating pressure derivatives for use in hydraulic test analysis. *Groundwater* 31, no. 5: 814–822.

Theis, C.V. 1935. The relation between the lowering of the piezometric surface and the rate and duration of discharge of a well using ground-water storage. *Eos, Transactions American Geophysical Union* 16, no. 2: 519–524.

Van Everdingen, A. 1953. The skin effect and its influence on the productive capacity of a well. *Journal of Petroleum Technology* 5, no. 06: 171–176.

Van Everdingen, A., and W. Hurst. 1949. The application of the Laplace transformation to flow problems in reservoirs. *Journal of Petroleum Technology* 1, no. 12: 305–324.

Walker, D.D., and R.M. Roberts. 2003. Flow dimensions corresponding to hydrogeologic conditions. *Water Resources Research* 39, no. 12: 1349.

Warren, J., and P.J. Root. 1963. The behavior of naturally fractured reservoirs. *Society of Petroleum Engineers Journal* 3, no. 03: 245–255.

Worthington, S., G.J. Davies, and D.C. Ford. 2000. *Matrix, fractures and channel components of storage and flow in a Paleozoic limestone aquifer*. In *Groundwater Flow and Contaminant Transport in Carbonate Aquifers*, ed. I.D. Sasowsky and C.M. Wicks, 113–128. Rotterdam: Balkema.

Xu, Z., B.X. Hu, H. Davis, and J. Cao. 2015. Simulating long term nitrate-N contamination processes in the Woodville karst plain using CFPv2 with UMT3D. *Journal of Hydrology* 524: 72–88.